Phase relations and hardness trends of ZrO_2 phases at high pressure

Yahya Al-Khatatbeh,[1] Kanani K. M. Lee,[1,2] and Boris Kiefer[1]
[1]*Department of Physics, New Mexico State University, Las Cruces, New Mexico 88003-8001, USA*
[2]*Department of Geology and Geophysics, Yale University, New Haven, Connecticut 06511, USA*
(Received 28 December 2009; revised manuscript received 6 May 2010; published 3 June 2010)

We use high-resolution synchrotron x-ray powder diffraction and density-functional theory (DFT) to investigate the phase stability, equations of state (EOSs), and mechanical hardness of zirconia (ZrO_2) up to ~54 and 160 GPa, respectively. For the equilibrium phase at ambient conditions (MI), we provide an experimental EOS that is comparable to results obtained from room-pressure Brillouin scattering experiments and bulk modulus-volume systematics but different from previous high-pressure experiments. The experimental second-order Birch-Murnaghan EOS parameters of MI-ZrO_2 are: ambient-pressure volume (V_0) of 35.15(±0.03) Å^3/f.u. with an ambient-pressure bulk modulus K_0 of 210(±28) GPa. For the high-pressure OI phase, we find that the K_0=290(±11) GPa, which is 19%–32% higher than previously determined, and V_0=33.65(±0.07) Å^3/f.u. The small volume decrease of 3.4% across the MI→OI transition at ~10 GPa is associated with a 38% increase in the bulk modulus consistent with our DFT calculations that predict a ~36% and 39% increase in K_0 for the generalized gradient and local density approximations, respectively. In contrast to the EOS of MI and OI, we find that our experimental EOS for the high-pressure OII phase is in good agreement with previous measurements. The large volume decrease across the OI→OII phase transition as obtained from both our experiments and calculations is ~10%. Our estimates, using scaling relations, indicate that this phase, while dense and quenchable, may have a comparatively low mechanical hardness of ~10 GPa.

DOI: 10.1103/PhysRevB.81.214102 PACS number(s): 81.40.Vw, 31.15.A−, 64.70.K−, 61.50.Ks

I. INTRODUCTION

The nature of bonding in transition-metal dioxide ZrO_2 is of interest as it has been considered to be hard, possibly a superhard material.[1–6] ZrO_2 is also involved in many industrial applications;[7–9] as such, ZrO_2 has been extensively investigated experimentally and theoretically under high pressure and/or high temperature.[1–3,5,6,10–17] The phase sequence at ambient temperature with increasing pressure is as follows: baddeleyite (MI, monoclinic, space group: $P2_1/c$) →orthorhombic I (OI, orthorhombic, space group: *Pbca*) →orthorhombic II (OII, orthorhombic, space group: *Pnma*).[1,5] At ambient pressure, two high-temperature phases of ZrO_2 have been found; namely a tetragonal (space group: $P4_2/nmc$) and a cubic (fluorite, space group: $Fm3m$) structure.[18,19] Additional tetragonal,[10] orthorhombic,[11] and hexagonal[12] phases of ZrO_2 have been reported at high pressures and/or high temperatures including two recently predicted phases for ZrO_2 with tetragonal (TET, space group: $P4/nmm$) and orthorhombic (OP, space group: *Pbcm*) structures.[4] Notably, the dense OII phase is observed to appear at pressures of ~12–25 GPa and can be quenched to ambient conditions.[1–3,6]

It is generally assumed that hardness increases with decreasing volume, either within a single phase, or across volume-reducing phase transitions.[20] As a result, quenchable high-pressure phases provide a promising route for the synthesis of mechanically stronger materials.[21,22] An implicit assumption is that the bulk modulus is a suitable proxy for the mechanical strength of a material.[23–25] However, systematics indicate that the bulk modulus may be a poor indicator of mechanical strength.[26,27] In contrast, the shear modulus may be a better estimator for the onset of plastic deformation but is more difficult to measure experimentally.[26,27]

The significantly denser OII phase has been suggested to be mechanically stronger than MI-ZrO_2 (Refs. 1–6): early measurements of the hardness of OII yielded values slightly higher than that of MI and the comparatively small increase was attributed to poorly-sintered and possibly phase-inhomogeneous samples, suggesting that the intrinsic hardness of the OII phase could be significantly higher.[28] Therefore, this phase has attracted great interest over the past 15 years with a particular focus on the equation of state, phase stability, quenchability, and the thermal (meta)stability at ambient pressure of OII-ZrO_2.[1–3,5,6,16] On the other hand, much less attention has been paid to the low-pressure phases MI and OI with respect to their stability and EOS.[1,11] As low-pressure phases are directly used in industrial applications, their physical properties (e.g., hardness, stability) provide important baseline values for the expected performance characteristics of high pressure phases. The EOS of MI-ZrO_2 has been measured repeatedly with bulk moduli at ambient conditions that range from 95 GPa (Ref. 11) to 212 GPa (Ref. 1). Bulk modulus-volume systematics give K_0 ~200 GPa in support of the higher value.[29] A larger bulk modulus is also supported by Brillouin scattering experiments (187–189 GPa).[30,31] Therefore, significant uncertainty exists in the compressional behavior of ZrO_2, even at low pressures.

In this study, we investigate the structural phase transitions of ZrO_2 up to a pressure of ~54 GPa at ambient temperature before and after laser heating to ~1800(±200) K. Furthermore, we employ *first-principles* DFT calculations to test stability and compressibility of ZrO_2. We estimate the hardness (H) of the experimentally observed ZrO_2 phases at ambient pressure directly from our computational results using a recently proposed scaling model.[32]

TABLE I. The experimental conditions for four runs on ZrO_2 samples. There are two unheated and two heated experiments at different pressures (22 and 40 GPa) to ~1800(±200) K. The stability range for the observed phases in each experiment is also given. For the heated experiments, all diffraction patterns were taken after cooling to room temperature.

Run	Heating history	Pressure measurement	Phase XRD observations	Pressure-quenched phases
1	Not heated	NaCl[a,b]	MI: 6–18 reflections from ~7 to 15 GPa; 1–3 reflections up to ~24 GPa (compression) OI: 1–3 from ~7 to 8 GPa; 5–10 reflections from ~9 to 28 GPa (compression) OII: 2 reflections at ~21 GPa; 5–11 reflections from ~24 to 50 GPa (compression); 8–11 reflections from ~50 to 0 GPa (decompression)	OII
2	Not heated	NaCl[a,b] and ruby[c]	MI: 8–29 reflections from ~2 to 15 GPa and 1–3 reflections up to ~24 GPa (compression) OI: One reflection from ~5 GPa; 5–15 reflections from ~8 to 27 GPa (compression) OII: 2 reflections at ~21 GPa; 5–11 reflections from ~24 to 42 GPa (compression); 9–11 from ~42 to 0 GPa (decompression)	OII
3	Heated to ~1800 K at ~22 GPa	NaCl[a,b]	MI: 4–19 reflections from ~9 to 16 GPa (compression, preheat); one reflection at ~22 GPa (compression, postheat); 6 reflections at 0 GPa (decompression, postheat) OI: 2 reflections at ~9 GPa (compression, preheat); 10–12 reflections from ~13 to 16 GPa (compression, preheat); 8–10 reflections ~22 to 25 GPa (compression, postheat) OII: 4–12 reflections from ~22 to 40 GPa (compression, postheat); 12–15 reflections from ~40 to 0 GPa (decompression, postheat)	MI and OII
4	Heated to ~1800 K at ~40 GPa	NaCl[a,b] and ruby[c]	OII: 8 reflections at ~35 GPa (compression, preheat); 9–10 reflections from ~40 to 54 GPa (compression, postheat); 8–9 reflections from ~54 to 0 GPa (decompression, postheat)	OII

[a]Reference 33.
[b]Reference 34.
[c]Reference 35.

II. EXPERIMENTAL METHODS

A polycrystalline sample of 99.7% ZrO_2 baddeleyite powder (Alfa Aesar, grain size: ~0.5–2 μm) was used as a starting material in our diamond-anvil cell (DAC) experiments. We performed four independent high-pressure DAC experiments to study the phase relations in ZrO_2 (Table I). In each experiment, our samples were mixed with sodium chloride (NaCl) that provided quasihydrostatic conditions and acted as a pressure calibrant[33,34] (ZrO_2:NaCl about 8:2 by mass). We also loaded 2 ruby spheres ~5–10 μm in diameter into the DAC to obtain a second independent pressure measurement.[35] The pressure as inferred from the ruby and/or the NaCl calibrants generally agreed to better than 4 GPa. The uncertainty in pressure was determined by averaging the measured pressures from NaCl and ruby. A rhenium (Re) gasket of an initial thickness of ~280 μm was precompressed to a thickness of ~35 μm. The sample and pressure calibrants were placed in a 150 μm hole in the center of the gasket and compressed between a pair of matched 300 μm culet diamonds. In two of the experimental runs, the sample was laser heated using an ~1 μm near-infrared laser for ~8 min up to ~1800(±200) K as determined by spectroradiometry.[36] Subsequently, the sample was temperature quenched and x-rayed at ambient temperature. While these experiments explore the *T*-quenched part of the high-*T* portion of the high-pressure phase diagram, we also collected angular-dispersive x-ray diffraction (XRD) at room temperature on cold compression and on decompression (Table I, Fig. 1). XRD patterns were obtained using a MAR345 image plate at the HPCAT beamline ($\lambda = 0.3875 \pm 1 \times 10^{-5}$ Å) at the Advanced Photon Source (APS) at Argonne National Laboratory, and at the CALIPSO[37,38] beamline ($\lambda = 0.4959 \pm 7 \times 10^{-5}$ Å) at the Advanced Light Source (ALS)

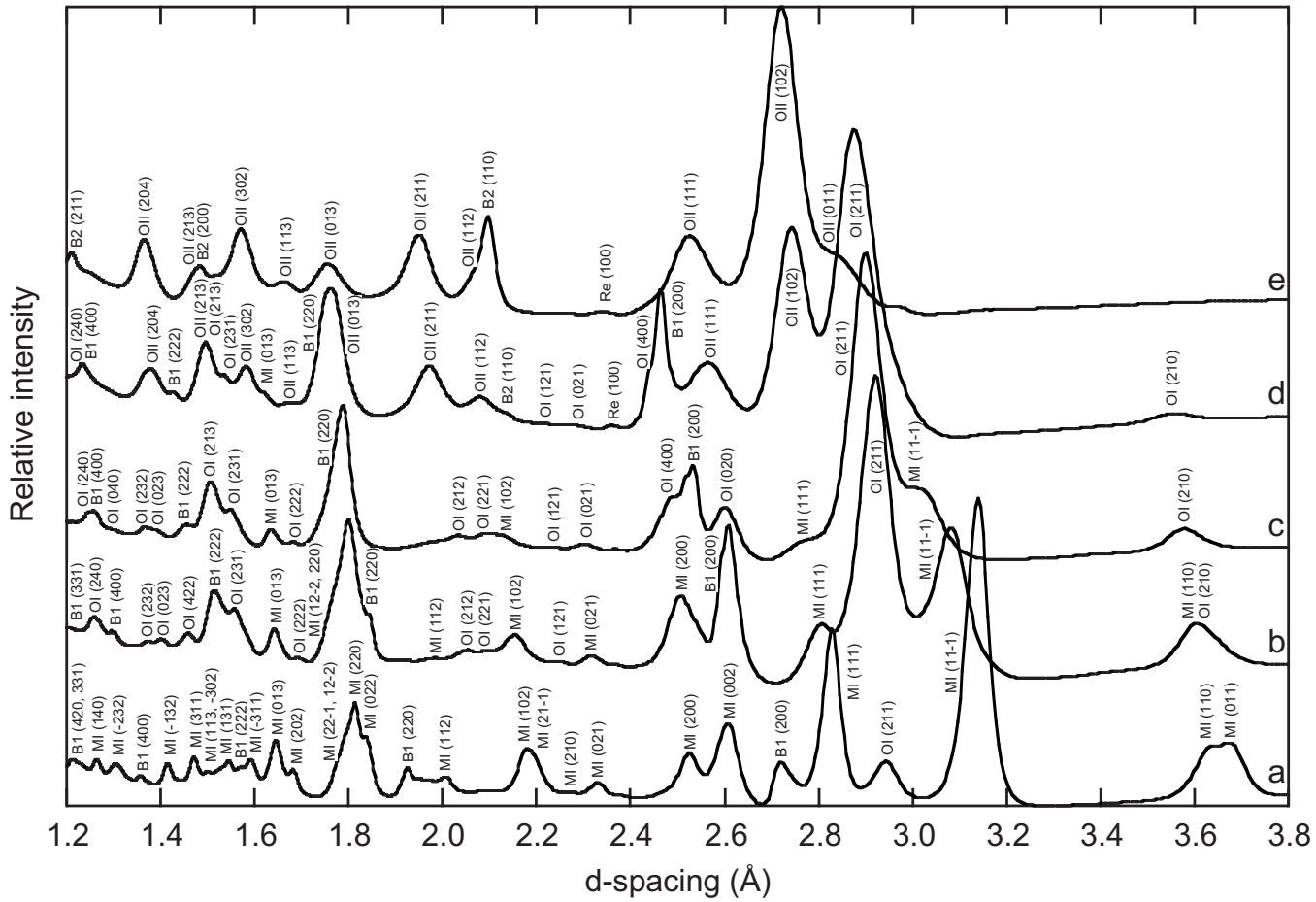

FIG. 1. X-ray diffraction patterns at various pressures during compression up to 42 GPa (run 2, unheated) taken at the CALIPSO beamline at the ALS show baddeleyite (MI), orthorhombic I (OI), orthorhombic II (OII), low-pressure phase NaCl (B1), and high-pressure NaCl (B2) corresponding Miller indices. A rhenium reflection from the gasket is marked with Re. Patterns shown are taken at the following pressures: (a) at 4.6 GPa, (b) at 11.8 GPa, (c) at 18 GPa, (d) at 26.2 GPa, and (e) at 42 GPa.

at Lawrence Berkeley National Laboratory. For heated experiments, samples were laser-heated at $22(\pm 1.2)$ and $40(\pm 0.1)$ GPa. Laser heating was used to anneal the sample and minimize deviatoric stress as well as to add a modest amount of thermal energy to the system to facilitate otherwise kinetically hindered phase transitions. This is particularly important in materials such as zirconia where the increasing coordination number requires formation of new bonds. All XRD measurements, whether laser heated or not, were taken at room temperature. One-dimensional patterns were obtained from the two-dimensional patterns by using the FIT2D software.[39] Volumes were determined using 5–12 reflections for MI, 5–9 reflections for OI, and 5–9 reflections for OII. A Birch-Murnaghan[40] EOS was used to determine the compressional behavior of the observed ZrO_2 phases. The third-order Birch-Murnaghan EOS is given by[40]

$$P = \frac{3}{2}K_0[(V/V_0)^{-7/3} - (V/V_0)^{-5/3}] \times \left\{1 + \frac{3}{4}(K_0' - 4)[(V/V_0)^{-2/3} - 1]\right\}, \quad (1)$$

where P is the applied pressure, V is the volume at pressure, V_0 is the room-pressure volume, K_0 is the room-pressure bulk modulus, and K_0' is the first pressure derivative of the bulk modulus at room pressure. From the thermodynamic relationship, $P = -\frac{\partial E}{\partial V}$, Eq. (1) can be integrated to obtain an expression for $E(V)$

$$E = \frac{9K_0V_0}{2}\left\{\frac{1}{2}[(V/V_0)^{-2/3} - 1]^2\right\} \times \left[1 + (K_0' - 4)\left\{\frac{1}{2}[(V/V_0)^{-2/3} - 1]\right\}\right] + E_0, \quad (2)$$

where E_0 is the energy at the ambient pressure volume. A second-order Birch-Murnaghan EOS is given by fixing K_0' to 4 in Eqs. (1) and (2). For both the experimental and theoretical data, ZrO_2 phases were fit using the second-order Birch-Murnaghan EOS.

III. THEORETICAL METHODS

To study the phase relations and the EOS of ZrO_2, our experiments were augmented with static *first-principles* calculations performed within the framework of density-functional theory.[41] Interactions between the atoms were

treated within the projected augmented wave (PAW) formalism,[42,43] core radii of 2.500 bohr (valence configuration: $4s^2 4p^6 5s^2 4d^2$) and 1.520 bohr (valance configuration: $2s^2 2p^4$) for zirconium and oxygen, respectively. Generalized gradient approximation (GGA) (Ref. 44) and local density approximation (LDA) (Ref. 45) were used to treat the electronic exchange- and correlation effects. The calculations were performed using the VASP software package[46] with an energy cutoff of 600 eV and centered k-point meshes.[47] Total energies were converged to better than ~1 meV/atom. In our calculations, we have used the following k-point meshes for the ZrO_2 phases: $4\times4\times4$ for MI, $2\times4\times4$ for OI, $4\times8\times4$ for OII, $6\times6\times8$ for TET, and $4\times4\times4$ for OP. We performed static calculations to determine the electronic ground state for each phase. During the geometry optimizations all internal degrees of freedom and lattice parameters were optimized simultaneously at fixed volume. The ground state energy for each phase was determined for 6–12 volumes, which encompass the experimental pressure range for each phase. All investigated ZrO_2 phases remain insulators throughout their stability ranges. The EOS parameters were obtained from the variation of the total energy with volume and fit to a second-order Birch-Murnaghan EOS[40] [Eq. (2) with $K_0'=4$].

The mechanical hardness of various ZrO_2 phases was estimated using a recently proposed scaling law that relates bond topology, electronic structure (charges of 4 and 6 used for Zr and O, respectively) and hardness in covalent and ionic materials.[32]

IV. RESULTS AND DISCUSSION

A. Experimental phase stability and equation of state

For all XRD patterns, all reflections are identified by NaCl, Re, or the three ZrO_2 phases MI, OI and OII (Fig. 1). Each ZrO_2 phase is described below.

1. Monoclinic baddelyite phase (MI)

MI was observed in the XRD patterns from ambient pressure at room temperature up to ~15 GPa (runs 1–3, Table I, Figs. 1 and 2). An x-ray reflection that can be attributed to the OI phase appears at ~4.6 GPa [run 2, Fig. 1(a)]. Comparable x-ray reflection strengths of these two phases occur in the pressure range of 8–12 GPa [Fig. 1(b)]; at higher pressure, OI x-ray reflections gain significant intensity over MI indicating a transition pressure of MI to OI as low as ~4.6 GPa, consistent with previous work,[1,11,15,48–50] although 1–3 reflections of MI were still observed up to ~22–24 GPa [Fig. 1(c)] and indicate a sluggish transition likely due to kinetics.

In run 3 (Table I), and in contrast to the other runs, MI was observed at ambient conditions in addition to the quenched OII phase, in agreement with previous observations.[6] For this run, the sample was heated at ~22 GPa and in Ref. 6 the sample was heated at 18.3 and 26.7 GPa. The room-pressure volume of the pressure- and temperature-quenched MI ($V_0=35.18\pm0.19$ Å^3), in excellent agreement with the initial value before compression (Table II).

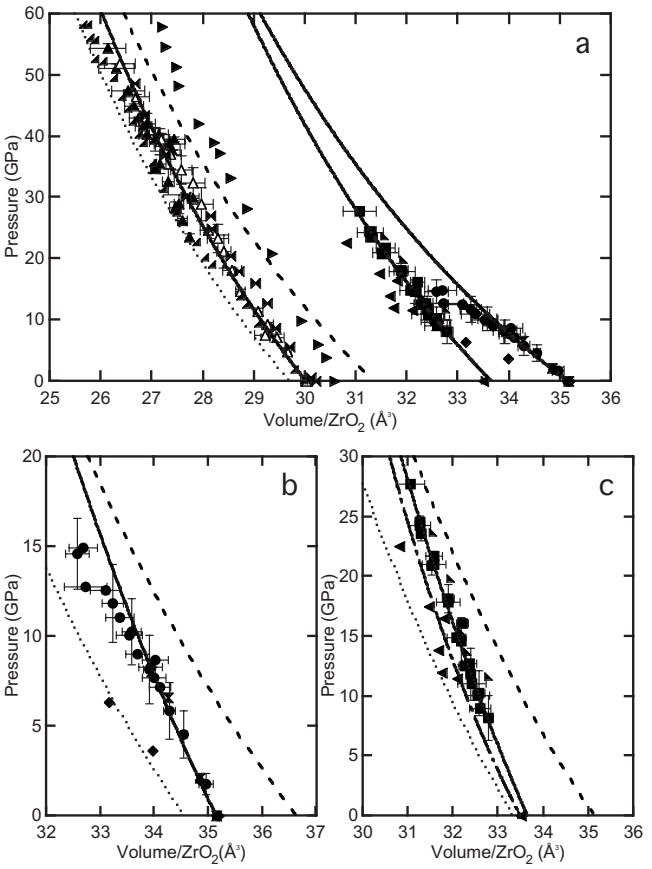

FIG. 2. Pressure versus volume of one ZrO_2 unit for MI (circles), OI (squares), and OII (triangles). The solid symbols indicate points under compression, and open symbols indicate points upon decompression. The solid curves indicate our EOS, whereas other curves show predictions based on LDA (dotted) and GGA (dashed) calculations. (a) All observed phases are shown and our observed OII are in good agreement with previous data (right-angled triangles for Ref. 3 and horizontal bowties for Ref. 6); however, the data of Ref. 1 (right-handed triangles) are shifted to larger volumes than our or other work. (b) MI: our data lie between our GGA and LDA calculations; for comparison, we list other experimental work (diamonds for Ref. 1 and vertical bowties for Ref. 11). (c) OI: our data lie between our GGA and LDA calculations; for comparison, we list other experimental work (left-handed triangles for Ref. 1 and inverted right-angled triangles for Ref. 11). The EOS curve of Ref. 11 (solid-dashed) does not fit either their data or ours.

The previously determined EOS of MI show large variations of the bulk modulus at ambient conditions: from 95(±8) GPa ($K_0'=4-5$) (Ref. 11) to 212(±24) GPa [$K_0'=8(\pm4)$] (Ref. 1) (Table II). In order to eliminate correlation between K_0 and K_0' and to compare BM-EOS values more directly, we fix K_0' to 4 for Ref. 1 and obtain $K_0=228(\pm10)$ GPa (Table II).[1] Additionally, the number of measurements taken for this phase in the previous studies[1,11] is small (four data points) compared to this study (18 data points), and our EOS curve goes through almost all of the data points [Fig. 2(b)]. To determine the EOS for MI from our data, a second-order Birch-Murnaghan EOS is fit to all points (18 points) up to ~15 GPa and K_0 is found to be 210(±28) GPa (Table II).

TABLE II. The equations of state of the ZrO_2 phases. The EOSs of MI and OII were obtained from a second-order Birch-Murnaghan equation of state [Eq. (1) with $K_0'=4$] to our experimental results in order to determine the isothermal bulk modulus (K_0). The EOS for OI was obtained from a (G versus g) second-order Birch-Murnaghan fit where zero-pressure volume per formula unit ZrO_2 (V_0) was determined (Refs. 40 and 52). For comparison, we list other experimental results (Refs. 1–3, 6, 11, 30, and 31). 1σ uncertainties are given in parentheses. For values not available, NA is recorded.

Phase	V_0 (Å^3)	K_0 (GPa)	K_0'	Reference
MI	35.15(0.03)	210(28)	4 (fixed)	This work (DAC+ADX)
	35.16	212(24)	8(4)	DAC+EDX,[a] reported values
	35.16	228(10)	4 (fixed)	DAC+EDX,[a] revised values[b]
	35.19	95(8)	4–5	DAC+ADX,[c] reported values
	35.06	187	NA	Brillouin scattering[d]
	35.06	189	NA	Brillouin scattering[e]
OI	33.65(0.07)	290(11)	4 (fixed)	This work (DAC+ADX)
	33.49	243(10)	7(2)	DAC+EDX,[a] reported values
	33.49	380(45)	4 (fixed)	DAC+EDX,[a] revised values[b]
	33.50	220	5 (fixed)	DAC+ADX,[c] reported values
	33.50	238(22)	4 (fixed)	DAC+ADX,[c] revised values[b]
OII	30.02 (0.11)	316(27)	4 (fixed)	This work (DAC+ADX)
	30.81	444(15)	1 (fixed)	DAC+EDX,[a] reported values
	30.59[f]	387(53)	4 (fixed)	DAC+EDX,[a] revised values[b]
	30.22(0.02)	332(8)	2.30(0.40)	DAC+ADX [g]
	30.03(0.08)	278(11)	3.70(0.22)	DAC+ADX [h]
	30	265(10)	4 (fixed)	MA+EDX [i]

[a]Reference 1.
[b]We have refit the data to the second-order Birch Murnaghan EOS to better compare results across studies.
[c]Reference 11.
[d]Reference 31.
[e]Reference 30.
[f]V_0 is taken from Fig. 5 given in this reference (Ref. 1).
[g]Reference 6.
[h]Reference 3.
[i]Reference 2.

Our measured bulk modulus K_{0T} of 210($\pm$28) GPa is in fairly good agreement with Brillouin scattering experiments[30,31] which measured an adiabatic bulk modulus K_{0S} value of 187–189 GPa. The difference between K_{0S} and K_{0T} is expected to be very small: the volume thermal expansion coefficient[51] of ZrO_2 at ambient pressure is $\alpha \sim 11 \times 10^{-6}$/K. Therefore, the difference between K_{0T} and $K_{0S}=K_{0T}(1+\gamma\alpha T)$, assuming $\gamma=1$, is estimated to be less than $\sim$0.3%, which is comparable with our measured value within the given uncertainties. Furthermore, the estimated bulk modulus for MI from bulk modulus-volume systematics is $\sim$200 GPa,[29] in support of our measured experimental K_0 value (Table II).

2. Orthorhombic phase (OI)

In the unheated experiments (runs 1 and 2, Table I), as mentioned above, OI reflections with significant intensities appear after $\sim$8 GPa [Fig. 1(b)], although 1–3 OI reflections can be observed at even lower pressures on compression, and as the pressure increases, the OI reflections become more intense than MI for pressures greater than $\sim$10 GPa [Figs. 1(c) and 2(c)]. At higher pressures ($P>15$ GPa), OI continues to gain intensity up to pressures of $P\sim21$ GPa, where two reflections of OII appear, and OI reflections remain up to 26–28 GPa [Figs. 1(d) and 2(c)]. Although two reflections of OII were visible at $\sim$21 GPa, comparable x-ray reflection strength between OI and OII begins at $\sim$24 GPa when OII becomes more intense and continues to increase in intensity up to $\sim$26–28 GPa [Fig. 1(d)].

In the heated experiments (runs 3 and 4, Table I), we have heated our samples at $\sim$22 GPa (run 3) and $\sim$40 GPa (run 4) to $\sim$1800($\pm$200) K. Starting at a pressure of $\sim$22 GPa (after heating), we observe x-ray reflections of OII in addition to OI and the strongest reflection from MI; in the pressure range 22–25 GPa, OI and OII x-ray reflections intensity become comparable. In none of our recovered samples, we observe OI.

Although the previously measured EOSs of OI (Refs. 1 and 11) are comparable to ours (Table II), there are some subtleties with the previous EOSs that warrant discussion. In Ref. 1, the EOS determination was based on only six data points, whereas we provide an EOS that is based on 20 data points [Fig. 2(c)]. When we plot the EOS curve given in Ref.

1 [Fig. 2(c)], it fits neither their data nor our data, indicating that there may be a mistake in the EOS determination and/or the data points plotted. In another study,[11] the small number of data points (seven data points) are scattered significantly [Fig. 2(c)] as compared to our measurements (20 data points). Using the G versus g formulation, the second-order Birch-Murnaghan EOS (Refs. 40 and 52) for this phase yields a V_0 of 33.65($\pm$0.07) Å^3/f.u., in good agreement with previous V_0 measurements,[1,11] and a K_0 =290($\pm$11) GPa, which lays in the significant range of bulk moduli reported previously (see Table II). Our measured bulk modulus value is larger than that of Ref. 11 but is based on more data points that cover the pressure range from ~8 GPa up to ~28 GPa [Fig. 2(c)].

3. Orthorhombic phase (OII)

In all experimental runs [Table I, Figs. 1(d), 1(e), and 2(a)], we observe OII x-ray reflections beginning at ~21–24 GPa on compression. In the unheated experiments (runs 1 and 2), OII is observed up to ~50 and 42 GPa (the highest pressures attained), respectively; and upon decompression from these pressures, OII remains visible in the x-ray patterns. In the heated experiments (runs 3 and 4), OII shows a similar behavior; i.e., it is the most abundant phase at pressures greater than 22 GPa up to the maximum pressure achieved under compression (40 GPa, run 3; 54 GPa, run 4) and could be recovered after decompression to ambient pressure.

The measured EOS of OII compares well with previous measurements [Table II, Fig. 2(a)][2,3,6] except for Ref. 1 as the given data points are shifted to larger volumes than observed in our and other previous work.[2,3,6] This also leads to a comparatively high bulk modulus of 444 GPa[1] which may be a result of the low K_0'=1. Fixing K_0'=4, the bulk modulus is lowered to 387 GPa, still significantly higher than other EOS determinations of OII-ZrO_2 (Refs. 2, 3, and 6) (Table II).

The experimentally observed volume change across OI $\rightarrow$OII transition is ~10.5% [Fig. 2(a)] in good agreement with previous measurements on ZrO_2 (Ref. 1) and similar oxides [e.g., HfO_2 (Ref. 1) and TiO_2 (Ref. 53)]. This large volume collapse indicates that OII is a dense phase and is observed to be the most stable phase at the highest pressure of our study of 54 GPa consistent with previous experiments.[1–3,6] As OII can be quenched to ambient conditions[1–3,6] and has a significantly smaller specific volume than either MI or OI (see Sec. IV C), it has been proposed that this phase is a superhard material (see Sec. III).[1–6,24]

B. First-principles computations: Phase stability and equation of state

In addition to the observed phases of ZrO_2 (discussed above), we have tested two recently proposed phases,[4] the TET and OP, and find that in agreement with our experiments and previous work,[1–3,6,11] the enthalpies are always higher as compared to the enthalpies of the experimentally observed phases (Table III, Figs. 2 and 3). We find that the transition from OII to TET is not likely to occur based on our enthalpy calculations and in agreement with Ref. 4. From our enthalpy calculations for both GGA and LDA approximations, the difference in enthalpy is large and corresponds to 0.14–0.20 eV/atom (Fig. 3) or an equivalent temperature of ~1600–2300 K, which indicates that TET may be a high-T phase, but if so, at temperatures greater than our peak temperatures of 1800($\pm$200) K.

Our computed LDA bulk moduli of ZrO_2 phases are in better agreement with the experimentally measured values, although it is ~27% and 26% lower for MI and OI, respec-

TABLE III. The calculated equations of state parameters of the ZrO_2 phases as obtained from our GGA and LDA calculations. Our calculations were fit to a second-order Birch-Murnaghan equation of state [Eq. (2) with K_0'=4] to find V_0 and K_0. For comparison, we list other theoretical results (Refs. 4 and 54–57) 1σ uncertainties are given in parentheses. For values not available, NA is recorded.

Phase	V_0 (Å^3)	K_0 (GPa)	K_0'	Reference
MI	36.64(0.04)	143(5)	4 (fixed)	GGA, this work
	34.55(0.04)	154(8)	4 (fixed)	LDA, this work
	35.62	138	NA	GGA[a]
	36.19	137	4 (fixed)	GGA[b]
	36.00	218	4.12	GGA[c]
	36.07	193	NA	GGA[d]
	34.17	184	4(fixed)	LDA[b]
	35.63	157	2.38	LDA[e]
OI	35.14(0.01)	195(2)	4(fixed)	GGA, this work
	33.33(0.02)	214(4)	4(fixed)	LDA, this work
	34.13	227	NA	GGA[a]
	34.69	204	4(fixed)	GGA[b]
	34.40	230	4.23	GGA[c]
	34.50	210	NA	GGA[d]
	32.97	236	4(fixed)	LDA[b]
	31.73	272	4.63	LDA[e]
OII	31.35(0.04)	251(3)	4(fixed)	GGA, this work
	29.70(0.02)	289(3)	4(fixed)	LDA, this work
	30.46	234	NA	GGA[a]
	30.86	251	4(fixed)	GGA[b]
	30.80	254	4.11	GGA[c]
	30.94	213	NA	GGA[d]
	29.24	298	4 (fixed)	LDA[b]
	29.41	305	4.68	LDA[e]
TET	32.53 (0.04)	214 (3)	4 (fixed)	GGA, this work
	30.61 (0.03)	256 (2)	4 (fixed)	LDA, this work
	31.59	192	NA	GGA[a]
OP	34.78(0.04)	159(3)	4 (fixed)	GGA, this work
	32.53(0.01)	190(4)	4 (fixed)	LDA, this work
	33.85	142	NA	GGA[a]

[a]Reference 4.
[b]Reference 54.
[c]Reference 55.
[d]Reference 56.
[e]Reference 57.

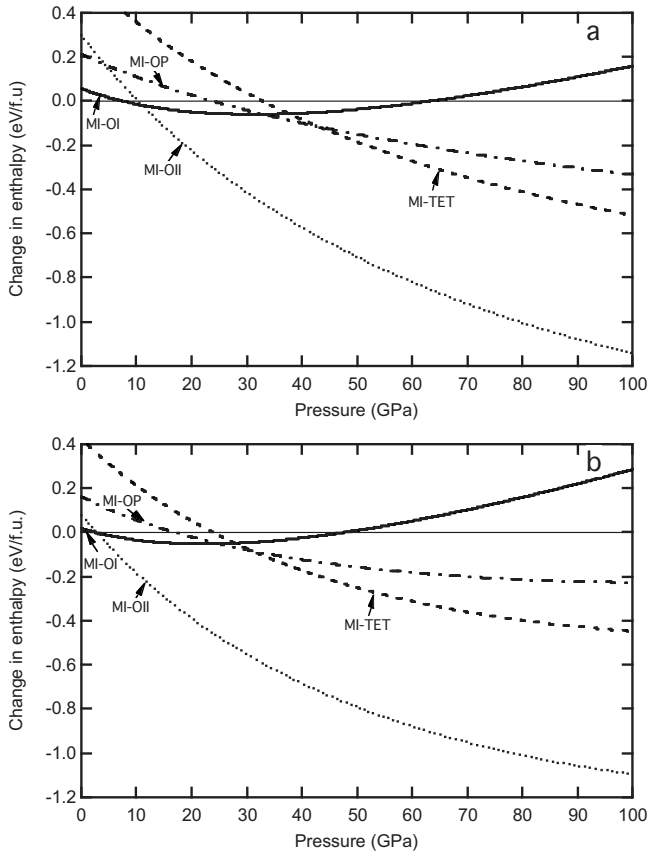

FIG. 3. Change in enthalpy with respect to MI versus pressure for various ZrO_2 phases for (a) GGA and (b) LDA. The difference in enthalpy curves with respect to MI is shown as MI-OI (solid), MI-OII (dotted), MI-OP (dashed-dotted), and MI-TET (dashed). Note the transition pressures for GGA: MI→OI at 7.5 GPa, OI→OII at 10.3 GPa. Likewise, the transition pressures for LDA: MI→OI at 2.5 GPa, OI→OII at 2.8 GPa. In both cases, the TET and OP phases have higher enthalpies.

tively (Tables II and III). The disagreement between experiment and theory for MI and OI phases may be explained by deviatoric stress resulting from the high-pressure conditions at room temperature. Only a few measurements of the OI phase and none of the MI phase occurred after laser heating when nonhydrostaticity is at a minimum. As all of the laser heating was done to synthesize the OII structure, suggests that this phase, although produced at the highest pressures in this study and others[2,3,6] and also includes measurements taken without any heating, may yield the most hydrostatic measurements thus yielding a closer value to the computations. However, our calculated EOSs are comparable to previous calculations using GGA (Refs. 4 and 54–56) and LDA (Refs. 54 and 57) (Table III). We speculate that the differences are at least partly due to the correlation of V_0 and K_0: As V_0 decreases, K_0 increases (Table III). However, these differences are more pronounced for the MI phase as the calculated K_0 in some references (184–218 GPa) (Refs. 54–56) is in good agreement with our measured high value (210(±28) GPa) and those estimated from bulk modulus-volume systematics (~200 GPa) (Ref. 29) and Brillouin scattering measurements (187–189 GPa) (Refs. 30 and 31) (Table II), which is significantly larger than our and most other previous calculations that range from 137 to 157 GPa (Refs. 4, 54, and 57) (Table III).

The predicted transition pressure from MI to OI to occur at 7.5 and 2.5 GPa using GGA and LDA, respectively, in good agreement with our experimental observations (Table I) and comparable with previous theoretical studies.[4,54] Additionally, the transition from MI to OI corresponds to an increase in bulk modulus of 36% and 39% for GGA and LDA, respectively (Table III), which is consistent with the measured increase of 38% across this transition (Table II). As for the OI→OII transition, our calculations give transition pressures of 10.3 and 2.8 GPa using GGA and LDA, respectively, which are lower than our experimental observations (Table I) but compatible with previous calculations.[4,54,55]

Finally, our calculated volume change across OI→OII transition is large and has values of 9.9% and 10.6% using GGA and LDA calculations, respectively, which compares well with our experimental observations as well as with previous experimental[1,2] and theoretical[4,54,55,57] works performed on ZrO_2 and similar dioxides.[53,54,58]

C. Hardness calculations

Currently available hardness values for the ZrO_2 system are measurements for the MI and OII phases. The measured hardness for the MI phase are 9.8 GPa (Ref. 59) and 13 GPa (Ref. 60) (Vickers hardness) and 11.6 GPa (Ref. 61) (Knoop hardness). The measured Knoop hardness for OII-ZrO_2 ranges from 11 to 17 GPa (Ref. 28) for samples quenched from 20 GPa and 800 °C. The authors of Ref. 28 noted that the pellets of the recovered samples were poorly sintered; the hardness range may reflect the coexistence of multiple phases[6] with different hardness values. Recently, two scaling laws, relating bond topology, electronic structure, and hardness, have been proposed.[32,62] For a wide range of materials, these models show good agreement in hardness values and are also in good agreement with available experimental observations: for example, the Vickers hardness of MI-ZrO_2 is predicted to be $H=10.8$ GPa (Ref. 62) in good agreement with measured values (Table IV).[59–61]

We use the Simunek and Vackar scaling model[32] to estimate the mechanical strength of the experimentally observed ambient temperature ZrO_2 phases. In this model, the hardness increases with decreasing average atomic volume, increasing average number of bonds per atom, decreasing coordination number, and decreasing average bond length.[32,63] In addition to crystal chemistry, the hardness depends also on the characteristic length scale (R_i) of the charge density distribution about each atom. These radii were determined iteratively such that the spatially integrated charge density within a spherical volume of radius R_i equals the number of valence electrons for each atomic species.[32] Using this method, we obtain $R(\mathrm{Zr})=1.82$ Å and $R(\mathrm{O})=1.08$ Å and $R(\mathrm{Zr})=1.78$ Å and $R(\mathrm{O})=1.08$ Å for GGA and LDA, respectively. We note that the implied ratio ($e_i=Z_i/R_i$) for oxygen, $e(\mathrm{O})=6/1.08=5.556$, is very similar to the independently derived value for oxygen in fluorite type TiO_2, $e(\mathrm{O})=5.964$.[64] In agreement with Refs. 32 and 63, we find that the radii do

TABLE IV. The calculated hardness of ZrO_2 using the Simunek and Vackar formalism (Ref. 32) considering the covalent model. In the given ZrO_2 phases, there are two oxygen sites (O1 and O2) as the average Zr-O bond length is different for each site. The average Zr-O1 distance is denoted by d_1 and Zr-O2 distance is denoted by d_2. CN is the coordination number of Zr atoms. For comparison, we list available experimental measurements for MI, OI and OII, along with values predicted (in italics) by the Simunek formalism (Ref. 63) for measured bond distances.

	Phase	CN	d_1 (Å)	d_2 (Å)	H (GPa)
GGA	MI	7	2.117	2.240	10.42
	OI	7	2.147	2.218	10.88
	OII	9	2.178	2.408	9.01
LDA	MI	7	2.093	2.193	11.64
	OI	7	2.116	2.179	12.07
	OII	9	2.134	2.359	10.10
Experiment	MI	7	2.090[d]	2.211[d]	9.8[a] 13[b] 11.6[c] *12.46*[e]
	OI	7	2.120[f]	2.190[f]	*12.98*[e]
	OII	9	2.145[h]	2.376[h]	11–17[g] *10.80*[e]

[a]Reference 59.
[b]Reference 60.
[c]Reference 61.
[d]Reference 65.
[e]Hardness values estimated using scaling relations discussed in Ref. 63 by using experimental d_1 and d_2 values given in Refs. 65, 17, and 5 in addition to our measured V_0 (Table II).
[f]Reference 17.
[g]Reference 28.
[h]Reference 5.

not depend strongly on phase; differences in radii between MI, OI and OII are less than 1.5%. The calculated hardness value of the MI phase, $H=10.4$ GPa (GGA) and $H=11.6$ GPa (LDA), compares well with available experimental values of 9.8–13 GPa (Table IV).[59–61] For the higher-pressure phases OI and OII, we find hardness values of 10.9 GPa (12.1 GPa) and 9.0 GPa (10.1 GPa) using the GGA (LDA). It is apparent that the hardness depends only weakly on phase and that the order of the estimated hardness values differs from the observed phase sequence in ZrO_2: $H(\mathrm{OII}) < H(\mathrm{MI}) < H(\mathrm{OI})$ (Table IV). Within the Simunek and Vackar scaling model,[32] this observation can be rationalized by analyzing the geometry dependence of the hardness: hardness increases with decreasing average atomic volume and decreasing bond length (for fixed coordination), as expected. However, the volume decrease is at least partially counteracted by an increasing coordination number and the associated higher electrostatic repulsion due to higher electric field gradients (Ref. 32). Zr is sevenfold coordinated in both MI and OI, and the specific volumes (Table II), and average bond lengths are similar. Thus, as expected the mechanical hardness of both phases are very similar (Table IV). In contrast, the specific volume collapse of ~10% across the OI → OII transition is compensated by the increase of the coordination number of Zr from 7 to 9, which leads to a lengthening of the shortest Zr-O bond and the two longest nearest-neighbor distances, thus increasing the average bond length by ~5%. The net effect of the specific volume decrease, bond length, and CN increase is to lower the hardness of OII below that of the OI phase (Table IV). However, the hardness values for MI, OI, and OII are very similar. As a result, if the two longest Zr-O bonds are excluded from the hardness calculation, we find that the hardness of OII increases by ~3 GPa. In summary, the assessment of the phase dependence of hardness in ZrO_2 depends strongly on crystal chemistry and nearest neighbor bond length distribution. However, the assessment that OII-ZrO_2 does not qualify as a superhard material is independent of the detailed treatment of the crystal chemistry.

Systematics suggest a correlation between shear modulus (G) and hardness; higher shear moduli correspond to a higher hardness.[26,27] Using the calculated elastic constants for the MI, OI, and OII-ZrO_2 phases,[56] we obtain for the Voigt-Reuss-Hill averages $G(\mathrm{OII};84.2\ \mathrm{GPa}) < G(\mathrm{MI};86.9\ \mathrm{GPa}) < G(\mathrm{OI};102.8\ \mathrm{GPa})$ consistent with the order of the predicted hardness values. On the other hand, our measured bulk modulus sequence (Table II) $K_0(\mathrm{MI};210\ \mathrm{GPa}) < K_0(\mathrm{OI};290\ \mathrm{GPa}) < K_0(\mathrm{OII};316\ \mathrm{GPa})$ shows an increase in bulk modulus with each higher pressure phase consistent with previous observations that the shear modulus is a better estimator for hardness values than the bulk modulus.[26,27] This analysis shows that it is unlikely that any of the currently known ZrO_2 phases qualify as superhard. In particular, experimental observations of the hardness of OII-ZrO_2 that were regarded as low and scattered due to poor sintering[28] may be a reflection of the low intrinsic hardness of this phase rather than related to sample preparation.

Furthermore, using scaling relations discussed in Ref. 63 and the experimental structure data at ambient conditions for MI,[65] OI,[17] and OII (Ref. 5) in addition to our measured ambient-pressure volumes (Table II), we find that the hardness values agree to within 2(1) GPa with the predicted GGA

(LDA) values obtained from *first-principles* calculations based on Simunek and Vackar model[32] (Table IV).

We would like to note that the weak dependence of hardness on phase is not universal and depends on the detailed changes in crystal chemistry (e.g., coordination number, specific volume, bond nature, and crystal structure) across a phase transition, as evidenced by the drastic increase of hardness across the graphite→diamond (Refs. 66 and 67) and quartz→stishovite (Refs. 60 and 68–71) phase transitions. Despite this difference, however, both systems still follow the correlation between increased shear modulus and increased hardness.[60,66–71]

V. CONCLUSIONS

We have studied the compressional behavior of ZrO_2 using both DAC experiments and DFT-based *first-principles* calculations. The stability range of each phase was studied to better understand the phase diagram of this dioxide and the high-pressure synthesis route of mechanically stronger materials. In this study, we provide a new experimental EOS for MI, although different from previous high-pressure experiments, provides a more reliable EOS that is comparable to results obtained from room-pressure Brillouin scattering experiments and bulk modulus-volume systematics. Furthermore, we find that the enthalpies of the recently proposed TET phase[4] is unlikely to appear in the ZrO_2 phase diagram at least at room temperature, consistent with our experiments at least up to ~1800(±200) K. Furthermore, our experiments show that the OII phase is stable up to at least 54 GPa, which is supported by our *first-principles* calculations. The magnitude of the observed and predicted volume collapse across the OI→OII transition is large. This finding as supported by both our experiments and calculations is in excellent agreement with the volume decrease across this transition in other isostructural dioxides.[1,53] Using scaling relations, OII-ZrO_2 is predicted to have a low mechanical hardness, comparable to MI and OI, thus confirming earlier hardness measurements on previously thought poorly sintered samples of OII.[28] This low mechanical strength is mainly due to an increased shortest Zr-O bondlength in the OII phase as compared to MI and OI. As a result, it is unlikely that any of the known ZrO_2 phases have a hardness in excess of 40 GPa, a prerequisite for a material to qualify as superhard.

ACKNOWLEDGMENTS

Portions of this work were performed at CALIPSO (XRD, laser heating) at the Advanced Light Source (ALS) at Lawrence Berkeley National Laboratory, and at HPCAT (XRD) at the Advanced Photon Source (APS) at Argonne National Laboratory. HPCAT is supported by DOE-BES, DOE-NNSA, NSF, and the W. M. Keck Foundation. APS and ALS are supported by the DOE. Y.A-K. and K.K.M.L. acknowledge support from CDAC. We also thank the beamline teams at CALIPSO and HPCAT beamlines for their cooperation and help; in particular, Simon Clark, Jinyuan Yan, Stanislav Sinogeikin, Yue Meng, and Daijo Ikuta.

[1] S. Desgreniers and K. Lagarec, Phys. Rev. B **59**, 8467 (1999).
[2] O. Ohtaka, H. Fukui, T. Kunisada, T. Fujisawa, K. Funakoshi, W. Utsumi, T. Irifune, K. Kuroda, and T. Kikegawa, Phys. Rev. B **63**, 174108 (2001).
[3] O. Ohtaka, D. Andrault, P. Bouvier, E. Schultz, and M. Mezouar, J. Appl. Crystallogr. **38**, 727 (2005).
[4] H. Ozturk and M. Durandurdu, Phys. Rev. B **79**, 134111 (2009).
[5] J. Haines, J. M. Leger, S. Hull, J. P. Petitet, A. S. Pereira, C. A. Perottoni, and J. A. H. da Jornada, J. Am. Ceram. Soc. **80**, 1910 (1997).
[6] J. Haines, J. M. Leger, and A. Atouf, J. Am. Ceram. Soc. **78**, 445 (1995).
[7] W. E. Lee and W. M. Rainforth, *Ceramic Microstructures: Property Control by Processing* (Champan and Hall, London, 1994).
[8] K. C. Patil, M. S. Hegde, T. Rattan, and S. T. Aruna, *Ceramic Microstructures: Property Control by Processing* (World Scientific, Singapore, 2008).
[9] K. Leinenweber, J. Mosenfelder, T. Diedrich, E. Soignard, T. G. Sharp, J. A. Tyburczy, and Y. Wang, High Press. Res. **26**, 283 (2006).
[10] H. Arashi, T. Yagi, S. Akimoto, and Y. Kudoh, Phys. Rev. B **41**, 4309 (1990).
[11] J. M. Leger, P. E. Tomaszewski, A. Atouf, and A. S. Pereira, Phys. Rev. B **47**, 14075 (1993).
[12] O. Ohtaka, T. Yamanaka, and T. Yagi, Phys. Rev. B **49**, 9295 (1994).
[13] C. J. Howard, R. J. Hill, and B. E. Reichert, Acta Crystallogr., Sect. B: Struct. Sci. **44**, 116 (1988).
[14] H. Boysen and F. Frey, Acta Crystallogr., Sect. B: Struct. Sci. **47**, 881 (1991).
[15] Y. Kudoh, H. Takeda, and H. Arashi, Phys. Chem. Miner. **13**, 233 (1986).
[16] O. Ohtaka, S. Kume, and E. Ito, J. Am. Ceram. Soc. **73**, 744 (1990).
[17] O. Ohtaka, T. Yamanaka, S. Kume, N. Hara, H. Asano, and F. Izumi, Proc. Jpn. Acad. **66**, 193 (1990).
[18] G. Teufer, Acta Crystallogr. **15**, 1187 (1962).
[19] D. K. Smith and C. F. Cline, J. Am. Ceram. Soc. **45**, 249 (1962).
[20] J. Z. Hu, H. K. Mao, J. F. Shu, Q. Z. Guo, and H. Z. Liu, J. Phys.: Condens. Matter **18**, S1091 (2006).
[21] J. Z. Jiang, H. Lindelov, L. Gerward, K. Stahl, J. M. Recio, P. Mori-Sanchez, S. Carlson, M. Mezouar, E. Dooryhee, A. Fitch, and D. J. Frost, Phys. Rev. B **65**, 161202(R) (2002).
[22] A. Zerr, G. Miehe, G. Serghiou, M. Schwarz, E. Kroke, R. Riedel, H. FueB, P. Kroll, and R. Boehler, Nature (London) **400**, 340 (1999).
[23] J. M. Leger, J. Haines, and B. Blanzat, J. Mater. Sci. Lett. **13**, 1688 (1994).
[24] J. M. Leger and J. Haines, Endeavour **21**, 121 (1997).
[25] J. E. Lowther, MRS Bull. **28**, 189 (2003).

[26] D. M. Teter, MRS Bull. **23**, 22 (1998).
[27] J. Haines, J. M. Leger, and G. Bocquillon, Annu. Rev. Mater. Res. **31**, 1 (2001).
[28] J. Haines, J. M. Leger, M. Schmidt, J. P. Petitet, A. S. Pereira, and J. A. H. da Jornada, in *Proceeding of the XXXIV EHPRG Conference*, edited by K. Heremans, (Leuven, Belgium, 1997), p. 13.
[29] O. L. Anderson, *The Nature of the Solid Earth* (McGraw-Hill, New York, 1972).
[30] M. V. Nevitt, S.-K. Chan, J. Z. Liu, M. H. Grimsditch, and Y. Fang, Physica B **150**, 230 (1988).
[31] S.-K. Chan, Y. Fang, M. H. Grimsditch, Z. Li, M. V. Nevitt, W. M. Robertson, and E. S. Zouboulis, J. Am. Ceram. Soc. **74**, 1742 (1991).
[32] A. Simunek and J. Vackar, Phys. Rev. Lett. **96**, 085501 (2006).
[33] Y. Sato-Sorensen, J. Geophys. Res. **88**, 3543 (1983).
[34] D. L. Heinz and R. Jeanloz, Phys. Rev. B **30**, 6045 (1984).
[35] H. K. Mao, J. Xu, and P. M. Bell, J. Geophys. Res. **91**, 4673 (1986).
[36] A. P. Jephcoat and S. P. Besedin, Philos. Trans. R. Soc. London, Ser. A **354**, 1333 (1996).
[37] M. Kunz, A. A. MacDowell, W. A. Caldwell, D. Cambie, R. S. Celestre, E. E. Domning, R. M. Duarte, A. E. Gleason, J. M. Glossinger, N. Kelez, D. W. Plate, T. Yu, J. M. Zaug, H. A. Padmore, R. Jeanloz, A. P. Alivisatos, and S. M. Clark, J. Synchrotron Radiat. **12**, 650 (2005).
[38] W. A. Caldwell, M. Kunz, R. S. Celestre, E. E. Domning, M. J. Walter, D. Walker, J. Glossinger, A. A. MacDowell, H. A. Padmore, R. Jeanloz, and S. M. Clark, Nucl. Instrum. Methods Phys. Res. A **582**, 221 (2007).
[39] A. P. Hammersley, S. O. Svensson, M. Hanfland, A. N. Fitch, and D. Hausermann, High Press. Res. **14**, 235 (1996).
[40] F. Birch, J. Geophys. Res. **57**, 227 (1952).
[41] P. Hohenberg and W. Kohn, Phys. Rev. **136**, B864 (1964).
[42] G. Kresse and D. Joubert, Phys. Rev. B **59**, 1758 (1999).
[43] P. E. Blochl, Phys. Rev. B **50**, 17953 (1994).
[44] J. P. Perdew, K. Burke, and M. Ernzerhof, Phys. Rev. Lett. **77**, 3865 (1996).
[45] J. P. Perdew and A. Zunger, Phys. Rev. B **23**, 5048 (1981).
[46] G. Kresse and J. Furthmuller, Phys. Rev. B **54**, 11169 (1996).
[47] H. J. Monkhorst and J. D. Pack, Phys. Rev. B **13**, 5188 (1976).
[48] A. S. Pereira, J. M. Leger, and J. A. H. da Jornada, Acta Metall. Mater. **42**, 2701 (1994).
[49] O. Ohtaka, T. Yamanaka, S. Kume, E. Ito, and A. Navrotsky, J. Am. Ceram. Soc. **74**, 505 (1991).
[50] S. Kawasaki, T. Yamanaka, S. Kume, and T. Ashida, Solid State Commun. **76**, 527 (1990).
[51] N. V. Bangaru and R. C. Krutenat, J. Vac. Sci. Technol. B **2**, 806 (1984).
[52] R. Jeanloz, Geophys. Res. Lett. **8**, 1219 (1981).
[53] Y. Al-Khatatbeh, K. K. M. Lee, and B. Kiefer, Phys. Rev. B **79**, 134114 (2009).
[54] J. E. Jaffe, R. A. Bachorz, and M. Gutowski, Phys. Rev. B **72**, 144107 (2005).
[55] R. Terki, G. Bertrand, H. Aourag, and C. Coddet, Mater. Sci. Semicond. Process. **9**, 1006 (2006).
[56] G. Fadda, L. Colombo, and G. Zanzotto, Phys. Rev. B **79**, 214102 (2009).
[57] J. K. Dewhurst and J. E. Lowther, Phys. Rev. B **57**, 741 (1998).
[58] J. Kang, E.-C. Lee, and K. J. Chang, Phys. Rev. B **68**, 054106 (2003).
[59] K. Takaoka, K. Hirota, M. Kato, O. Yamaguchi, and S. Ohtaka, J. Soc. Mater. Sci. Jpn. **55**, 258 (2006).
[60] J. H. Westbrook and H. Conrad, *The Science of Hardness Testing and Its Research Applications* (ASM, Ohio, 1973).
[61] C. M. Sung and M. Sung, Mater. Chem. Phys. **43**, 1 (1996).
[62] F. Gao, J. He, E. Wu, S. Liu, D. Yu, D. Li, S. Zhang, and Y. Tian, Phys. Rev. Lett. **91**, 015502 (2003).
[63] A. Simunek, Phys. Rev. B **75**, 172108 (2007).
[64] Y. Liang, B. Zhang, and J. Zhao, Phys. Rev. B **77**, 094126 (2008).
[65] D. K. Smith and W. Newkirk, Acta Crystallogr. **18**, 983 (1965).
[66] J. R. Patterson, S. A. Catledge, Y. K. Vohra, J. Akella, and S. T. Weir, Phys. Rev. Lett. **85**, 5364 (2000).
[67] R. A. Andrievski, Int. J. Refract. Met. Hard Mater. **19**, 447 (2001).
[68] J. M. Leger, Nature (London) **383**, 401 (1996).
[69] H. J. McSkimin, P. Andreatch, and R. N. Thurston, J. Appl. Phys. **36**, 1624 (1965).
[70] B. Holm and R. Ahuja, J. Chem. Phys. **111**, 2071 (1999).
[71] D. J. Weidner, J. D. Bass, A. E. Ringwood, and W. Sinclair, J. Geophys. Res. **87**, 4740 (1982).